The Application of a Scanning, Water Raman-Lidar as a Probe of the Atmospheric Boundary Layer

William E. Eichinger, Daniel I. Cooper, Marc Parlange, and Gabriel Katul

Abstract—**A scanning water Raman-lidar has been designed and constructed to study surface–atmosphere processes with high spatial and temporal resolution. Analytical methods are also being developed to analyze the information this lidar can take. The lidar is able to measure the absolute water content and then calculate evaporative fluxes and other atmospheric parameters quickly over relatively large areas. This capability provides new opportunities for the study of microscale atmospheric processes. Examples of data and analyses are presented. An analysis is presented which determines the spatial and temporal resolution which is required of a remote sensor in the boundary layer.**

I. Introduction

THERE is a growing body of observational and theoretical evidence which suggest that energy budget and hydrological variables are associated with variations in the Earth's surface [1]–[3]. This link between surface variability and local scale processes must made if we are to improve our understanding of the feedback mechanisms involved in surface–atmospheric dynamics. Similarly the interaction of the surface and the lower atmosphere is intimately involved with the development of the local climate and must be included in regional scale models. However, to understand these interactions, the surface–atmosphere interface must be studied as a large-scale spatial system.

Traditional approaches used to measure surface–atmosphere processes include the Bowen ratio technique, which requires estimates of the vertical gradient of water vapor and temperature, and eddy correlation techniques, which measure the covariance of the moisture content or temperature, and vertical wind speed at a single location. There are several difficulties in making these types of measurements. The first is that these instruments cannot measure atmospheric parameters and fluxes accurately under all types of atmospheric conditions [4]. Another limitation common to all point instrument approaches is the assertion that measurements at a single location represent the properties of a larger region. This assertion is based upon assumptions of horizontal homogeneity and the validity of Taylor's Hypothesis. These assumptions may not be true even in ideal situations [5]. As will be shown, there is evidence which indicates that a point measurement is representative of an area less than 10 m in radius (varying with local conditions) which may or may not be related to the local average. Conventional techniques require long averaging times and thus cannot address temporal variability. Lastly, conventional point sensors are inappropriate for use in complex terrain or varied vegetation where the assumptions of stationarity and horizontal homogeneity cannot be made. Unfortunately, these conditions are precisely those which are likely to have the greatest impact on local climate.

To address issues of temporal and spatial variability, Los Alamos National Laboratory has developed a water-vapor remote sensing capability to study evapotranspiration (ET). Specifically, a scanning, water Raman-lidar (light detection and ranging) has been designed and built. A lidar of this type is an ideal tool to study spatial atmospheric properties. It is a noninvasive technique which can measure the water vapor concentration rapidly over relatively large areas with high spatial resolution. The ability to map the water vapor concentration enables the measurement and visualization of turbulent structures and microscale processes in the inner region of the boundary layer. Data from the Raman lidar has been used by the Los Alamos staff and their collaborators to examine spatial and temporal variations of water vapor concentrations and fluxes, the spatial and temporal power spectra of turbulent structures, to determine turbulence cell size distributions, the Monin–Obulkov stability length, and the atmospheric stability correction functions. Current work also includes a statistical examination of lidar data to determine the applicability of many common assumptions such as stationarity, homogeneity, ergodicity, and Taylor's Hypothesis.

This paper will summarize the methodology for the analysis of lidar data to determine meteorological parameters. The techniques shown here are not exhaustive but will show the depth and breadth of the information which can be obtained from the lidar scans. An analysis will be shown which determines the spatial and temporal resolution required of a remote sensor if it is to study turbulence in the boundary layer of the atmosphere.

II. Lidar Description

The scanning, solar-blind water Raman-lidar used in this experiment was built at Los Alamos and is based upon the techniques pioneered by Melfi *et al.* [6] and Cooney [7]. Details of this instrument are described by Eichinger *et al.* [8]. The system has evolved considerably since the original experiments in 1990. The current lidar system parameters are outlined in Table I. This mobile, truck-mounted lidar system is totally self-contained, including its own analysis and control computers and electric power generator. A distinctive aspect

Manuscript received February 26, 1992; revised July 16, 1992. This work was supported by the Department of Energy, Office of Health and Environmental Research.

W. E. Eichinger and D. I. Cooper are with the Los Alamos National Laboratory, Los Alamos, NM 87545.

M. Parlange and G. Katul are with the Department LAWR, University of California, Davis Campus, Davis, CA 95616.

IEEE Log Number 9204859.

TABLE I
CURRENT LIDAR OPERATIONAL PARAMETERS

Wavelength:	248-nm
Energy per Pulse:	0.4 J
Maximum Laser Pulse Rate:	250 Hz
Laser Beam Divergence:	2-mrad
Telescope:	40.6-cm, f/8 Cassegrain
Detector:	Photomultipliers, Thorne EMI 9813QB
Signal:	273-nm N_2 Raman Scatter
	263-nm H_2O Raman Scatter
Filters:	3-nm wide, ≈10% transmission
Digitizers:	LeCroy 8818, 100-Mhz, 8-bit
Nominal Range Resolution:	3.0-m
Scanner Angular Resolution:	0.5 mrad
Maximum Effective Range:	≈ 450-m

of this instrument is that the signal from the returning light is digitized directly rather than relying primarily on photon counting for most of the range as is the custom with most Raman lidars. While this limits the range, it enables high spatial resolution (1.5 m) data elements and the application of rapid scanning techniques. Pulses are summed to increase the signal-to-noise ratio (SNR) along each line of sight. The number of pulses considered to have the minimum acceptable SNR is dependant upon the desired range, and laser energy per pulse and varies from 5 to 25. The time required to take and save each summed data set from a single line of sight also varies from 0.12 s to several seconds.

A Lambda Physics EMG 203 MSC excimer laser operating at 248 nm (KrF) is used as the laser source. The laser beam is aligned so that it is coaxial to the optical axis of a 40.6-cm diameter f/8 Cassegrain telescope. Using a periscope mirror assembly mounted at the exit of the telescope, the system is able to scan 75° horizontally and up to 27° above horizontal. The return signal from both atmospheric nitrogen and water vapor is digitized directly. Because nitrogen is the dominant atmospheric gas, dividing the water Raman return signal by that of nitrogen normalizes each pulse and corrects for first-order atmospheric transmission effects, variations in laser energy from pulse to pulse and telescope field of view overlap with the laser beam. The divided returns are then directly proportional to the absolute water vapor content of the air and require only a correction for differential ozone absorption at the two return wavelengths. This correction is measured by calibrating the lidar at regular intervals out to the maximum range using a assman psychrometer. As the range increases, the apparent water concentration rises because of the greater attenuation of the nitrogen signal. The exponential correction factor has varied between 0.0 and 0.00091 m^{-1} and has not been observed to vary more than 15% during the course of an experiment.

In all of the lidar experiments an array of micrometeorological instruments are used as a reference set. Included in these instruments are Campbell Scientific Inc. dew-point hygrometer Bowen Ratio Energy Balance (BREB) systems and eddy-correlation (EC) systems. Soil heat flux plates, net radiometers, a three-dimensional sonic anemometer, a sensitive weighing lysimeter, an array of neutron probe access tubes, and a time-domain reflectometer have also been included in the instrument array.

The calibration of a fast scanning lidar is a unique problem. Conventional water vapor sensors fall into two general categories. The first category is capable of measuring the absolute water concentration and includes devices such as capacitance hygrometers and psychrometers. Because the time constant for these devices ranges from 20-s to 180-s (depending on the type of device and the degree to which the housing restricts the airflow), the time resolution of the lidar must be greatly degraded in order to compare values within the same time domain. Fig. 1(a) is a comparison of lidar water concentrations and those from this category of instruments where the lidar time resolution has been degraded to match the instrument. The second category of instruments includes devices capable of fast time response, but are incapable of absolute water concentration measurements. Krypton hygrometers are a common example of this category. Because of the difficulty in obtaining an absolute concentration with these devices, we have avoided direct comparison with this type of device. While comparisons to psychrometers provide valuable calibration data for the lidar, they are incapable of determining the ability of the lidar to accurately track transient water concentrations. Fig. 1(b) is a comparison of lidar water concentrations and capacitance hygrometer concentrations in which the lidar time resolution has not been degraded. The agreement between the two instruments is clearly not as good. This is due to the greater than 20-s time constant of the capacitance hygrometer and its resultant inability to track water vapor fluctuations on the order of a second or less. Furthermore, all conventional sensors measure at a finite point, or at best have a footprint oriented into the mean wind. Whereas the lidar measures not only in time but in space as well. Thus comparisons with point sensors are limited by the incompatible spatial dimension as well. An additional related problem in calibration is that many conventional instruments cannot resolve low water vapor concentrations (less than 20% humidity) and may differ by factors of five in this moisture regime [9].

The lidar system can be programmed to execute a number of different types of scanning strategies varying from single or multiple laser shots along a single line of sight to three dimensional scans. The most commonly used scans are two-dimensional horizontal or vertical "slices" of the water vapor concentration over an area, and what we call time domain (TD) scans because they were taken to directly compare temporal and spatial data. Two-dimensional scans are made by taking multiple lasers shots along several lines of fight at constant azimuth or elevation. The speed at which this can be completed depends on the number of lines of sight and the number of shots taken at each angle. It is possible to complete a horizontal scan over a 45° field of view with 0.5° increments in 51 s.

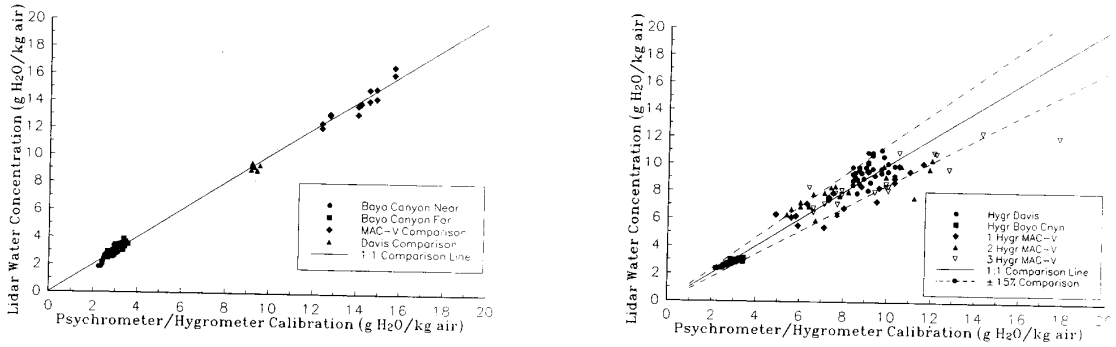

(a) (b)

Fig. 1. Comparison of lidar water vapor concentrations with those from conventional psychrometers and capacitance hygrometers. Fig. 1(a) contains data in which the lidar time resolution was degraded to match that of the comparison instrument. Fig. 1(b) contains data in which the lidar time resolution was not degraded. The apparent variations in Fig. 1(b) are due to the long (> 20-s) time constant of the capacitance hygrometer and its inability to track water vapor fluctuations on the order of a second or less.

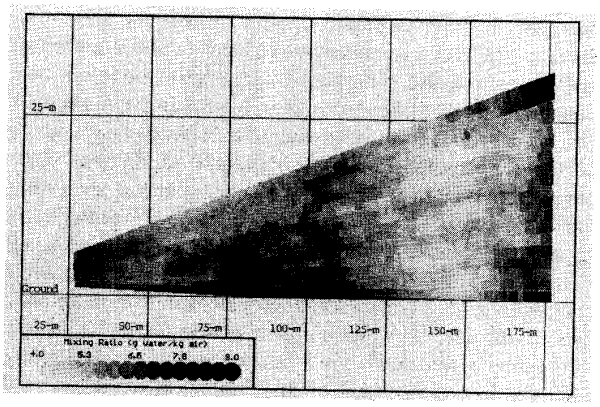

Fig. 2. An example of a vertical water vapor concentration profile taken by the lidar. Note the dry areas at 50-m and 150-m and the relatively wet areas from 75-m to 125-m. These are examples of plume-like structures which show why fluxes and concentrations are so variable.

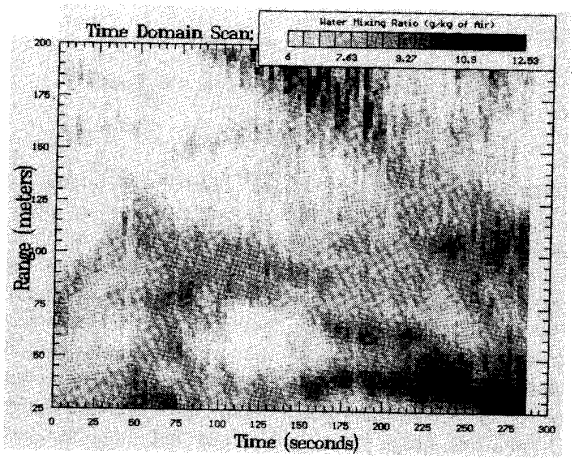

Fig. 3. An example of a Time-Dimensional (TD) scan taken over a uniform alfalfa field at Maricopa. This plot shows the variations in water vapor concentrations along one line of sight as a function of time. Water vapor concentrations are not uniform in space or time by factors of nearly two.

Fig. 2 is an example of a scan of this type. In TD scans, the laser is fired along a single line-of-sight parallel to the ground. A given number of laser pulses were summed, saved to computer hard disk, and the process repeated until the available computer disk space was filled. Each series of one-dimensional scans taken in this manner creates a two-dimensional array of values. The values in each column represent the water vapor concentration at a given time at various distances from the lidar, whereas the values in each row represent the water vapor concentrations at a given distance from the lidar as a function of time (Fig. 3). Data of this nature allows the direct comparison of temporal and spatial information. Because of the number of scans and the relatively long distances involved, the number of useful data points approaches one-half million, enabling comparisons of high statistical significance. Because the number of laser pulses that were summed varied from 5 to 100, the rate at which spatial data sets were generated varied from 0.11 s to 10.6 s, and the length of the time series varied from 2 to 20 min.

The nature of the time domain (TD) data argues for short summing times taken over as long a period as possible in order to examine the spatial and temporal change in detail. However, two- and three-dimensional scans should be done fast enough to capture atmospheric processes in motion. If the scan takes too long to accomplish, the atmosphere could change significantly during that time. This desire must be balanced by the reality that a larger number of laser pulses summed together increases the effective range. Thus there will always be some distortion caused by air motion during the scan. This effect has been studied in some detail and has resulted in a rule of thumb that the scan speed should not be less than 0.3° per second. This rate will give acceptable results at wind speeds of 4 to 5 m per second during the midday when flux rates are highest. At night or during calm wind conditions, this requirement can be relaxed.

III. Experimental Tests

Three major experimental tests of the system have been performed. The first was a local test in Bayo Canyon, Los Alamos County, NM, which was to test the ability of the lidar to duplicate the measurements of standard point instruments. The

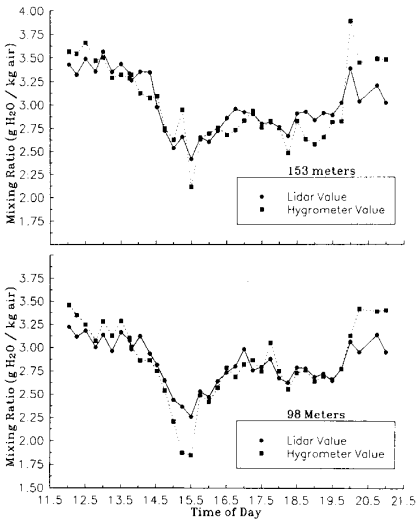

Fig. 4. A comparison of lidar-derived water vapor mixing ratios and those derived from capacitance hygrometers at two ranges from the lidar. The data from both instruments has been averaged over a 100-s interval to approximate the response time of the hygrometers. The experiment took place in Bayo Canyon, Los Alamos County, NM.

second experiment took place in Maricopa, AZ was the first full system test including scanning. The system was again improved for a third experiment at the University of California, Davis.

In the Bayo Canyon experiment, capacitance hygrometers were placed at distances of 98 and 153-m from the lidar. Every 15 min the lidar took a 100-s average along a line of sight past the two hygrometers. Data from both the lidar and the hygrometers were averaged over 100-s to approximate the response time of the hygrometers. The results are shown in Fig. 4. The root-mean-square (rms) difference between the water vapor mixing ratio as determined by the hygrometers and the lidar is 0.12 g-water/kg-air, corresponding to approximately a 5% difference. In all cases, the lidar measured value lies within the range of values measured by the hygrometer during the sampling period. Further comparisons between the lidar and conventional instrumentation also show good correlation. During the Maricopa experiment, the lidar measured mixing ratio was compared and calibrated with an Assman psychrometer at various ranges out to 450-m. The rms difference in measurements in that case was 0.3 g water/kg air, corresponding to a 3% difference.

The first experiment designed to test the scanning capabilities of the lidar and begin evaluating concepts for flux determination took place at Maricopa, AZ in June of 1990, as part of the fifth Maricopa Agricultural Center field campaign (MAC-V). A unique aspect of this experiment was the relatively dense array of point instruments in the field at the same time. The vegetation at the site consisted of uniform alfalfa, in a laser-leveled irrigation basin which had been flooded 5 days prior to the experiment. At the time of the experiment, the alfalfa was 80-cm tall and the field extended at least 1 km in the predominant upwind direction.

The third experiment took place at the Campbell Tract of the University of California, Davis Campus in August, 1991. Again, the experiment included a relatively dense array of point instruments. The Davis site consisted of an irrigated bare field in a larger dry, bare field surrounded by irrigated fields of beans, grass and corn. The experiment incorporated several improvements to the scanning capabilities of the lidar and the scanning strategies including a 250-Hz laser. While the energy of an individual laser pulse was decreased, the ability to take more pulses at a faster rate made up for the difference. This experiment is intended to show the ability of the instrument to perform comprehensive atmospheric measurements and analysis. The variations in canopy and roughness length at the Davis site allows a unique opportunity to study the concept of fetch and to measure the growth of the boundary layer. The data analysis for this experiment is continuing.

IV. Data Analysis Techniques

Two methods for flux computation will be described. The first uses the fact that the water vapor concentration in the vertical direction follows a logarithmic profile when corrected for atmospheric stability. The slope of this profile is directly proportional to the water vapor flux [10], [11]. The second method involves using inertial dissipation techniques in which lidar-derived spatial and temporal power spectra are used to determine the flux [10]. It is worth noting that the techniques shown here can be applied to measure the fluxes of any atmospheric scalar and do not require high-speed scanning techniques. For example, a temperature measuring lidar could apply this model to measure the sensible heat flux. Similarly, a lidar capable of measuring the carbon dioxide concentrations could use the same model to determine the flux of carbon dioxide from a plant canopy.

Monin–Obukhov similarity theory can be used to compute surface fluxes from profiles of water vapor concentration, temperature, and windspeed within the inner region of the boundary layer. The inner region is defined by a fully developed turbulent atmosphere that has a stationary and horizontally uniform boundary layer. The profile equation for the stability corrected mean water vapor concentration is

$$\overline{q_s} - \overline{q}(z) = \frac{E}{a_v k u * \rho}\left[\ln\left(\frac{z-d_0}{z_{0v}}\right) - \Psi_{sv}(\zeta)\right] \quad (1)$$

where

- a_v the ratio of Von Karman's water vapor constant to Von Karman's constant ≈ 1.0,
- k Von Karman's constant [≈ 0.40],
- d_0 the displacement height [m],
- E the water vapor flux $[\mathrm{kg/m^2 s}]$,
- L the Monin–Obukhov length [m],
- $\overline{q_s}$ the mean water mixing ratio at the surface [kg/kg],
- $\overline{q}(z)$ the mean water mixing ratio at height z [kg/kg],
- u^* the friction velocity [m/s], (vertical momentum per unit mass)
- z the measurement height [m],
- z_{0m} the roughness length for momentum [m],

z_{0v} the roughness length for water vapor [m],
ρ density of the air [kg/m^3],
$\Psi_{sv}(\zeta)$ the diabatic correction for water vapor
for unstable, $\zeta < 0$, conditions,

$$= 2\ln[(1+x^2)/2], \tag{2}$$

for stable, $\zeta > 0$, conditions,

$$= 5.2\zeta, \tag{3}$$

x $(1-16\zeta)^{.25}$,
ζ the Monin–Obukhov dimensionless variable
$= (z-d_0)/L$.

Rearranging (1) into linear form and assuming that the logarithmic profile for water vapor holds for "instantaneous" measurements

$$q(z) = -Mz' + b \tag{4}$$

where

M is the slope of the fitted function $M = E/a_v ku * \rho$,
$q(z)$ is the mixing ratio at height z [kg/kg],
z' is the reduced height parameter $z' = \ln(z-d_0) - \Psi_{sv}(\zeta)$,
b is a regression constant $b = M\ln(z_0) + \overline{q_s}$.

If the vertical profile of the atmosphere at a given point in space is measured, and a least squares line is fitted using (4), then the flux is defined as

$$E = Ma_v ku * \rho. \tag{5}$$

Lidar measured vertical profiles of water vapor concentration taken by scanning in the vertical direction require u^*, L, and air density measurements from standard meteorological instruments to estimate the water vapor flux. A lidar vertical scan has the property of making a series of measurements at many heights over distances of several hundred meters. The concentrations at all heights in a given range interval are assumed to be at a single range and are used to fit (4). When spatial averaging such as this is performed, the lidar derived values converge quite well to the logarithmic model. When distances as short as 5 to 10 m are spatially averaged, they show convergence to the model. This is fortuitous in that it enables flux measurements at many locations along the line of sight. Multiple vertical scans along several different azimuths allows for flux mapping over an area. A unique aspect of the lidar method is that in fitting a relatively large number of data points, one can calculate the degree to which the data fits the model, and thus estimate the uncertainty. This is in contrast to methods such as Bowen Ratio which fits a similar model with only two points.

By fitting the lidar data to the model using (2)–(4) with least-squares curve fit, both the Monin–Obulkov stability length, L, and the gradient of the profile can be found. Due to the complexity of the calculation, an iterative method must be used. This technique provides a valuable measure of atmospheric stability.

Through an analysis of the spatial power spectra with dissipation techniques, the water vapor flux can be determined. Champagne *et al.* [12] were the first to use this property to derive fluxes from temporal spectra from point instruments which was converted to spatial spectra by virtue of the wind speed. With a lidar, fluxes can be derived from either the spatial or temporal spectra directly.

In a turbulent flow, large eddy structures break down into increasingly smaller eddies. At some point, the eddies become small enough for viscous effects to become important, and at that point the turbulent energy is dissipated as heat. The scale over which atmospheric structures break down from larger to smaller sizes without loss of energy is known as the inertial subrange. This range generally spans several orders of magnitude and extends down to the Kolmogorov scale—approximately 1 mm. Based upon dimensional analysis, Kolmogorov [13] argued that the power spectrum of the wind speed in the inertial subrange region is a function of wavenumber, κ, and should be proportional to $\kappa^{-5/3}$. Corrosin [14] derived the form for spatial temperature power spectra which is applicable to water vapor concentration by similarity. The spatial power spectral equation for water vapor has the following form:

$$F_q(\kappa) = \beta q \epsilon^{1/3} \epsilon_q \kappa^{-5/3} \tag{6}$$

The power spectrum is normalized by:

$$\int F_q(\kappa)\, d\kappa = \bar{q}^{2} \tag{7}$$

where

$\bar{q}^{2}$ = the average variance of the water vapor concentration,
β_q = the Kolmogorov constant [≈ 0.80] (believed to be constant for all scalars),
ϵ = the turbulent energy dissipation rate [m^2/s^3],
ϵ_q = the dissipation rate due to molecular diffusion $1/2\ \partial\bar{q}^{2}/\partial t$, [1/s],
κ = the wavenumber [1/m].

Two additional relationships are also required to solve for the flux:

$$\epsilon_q = \frac{E^2 \Phi_{sv}(\zeta)}{\rho^2 u * k(z-d_0)} \tag{8}$$

$$R_m = \frac{k(z-d_0)\epsilon}{u*^3} \tag{9}$$

where

$\phi_{sv}(\zeta)$ = the water vapor diabatic stability gradient,
for unstable, $\zeta < 0$, conditions $= (1-16\zeta)^{-0.5}$,
for stable, $\zeta > 0$, conditions, $= 1.0 - 5.2\zeta$.
R_m = a dimensionless scaling function,

A number of parameterizations exist for the scaling function R_m. We have found the one developed by Busch and Panofsky [15], and Garratt [16] to give the best results. This parameterization is based upon theoretical arguments that the rate of energy dissipation of turbulent kinetic energy, ϵ, must equal the rate of energy production by shear stress and buoyancy.

The following expression is used:

$$R_m = \Phi_m(\zeta) - \zeta$$

where

Φ_m = the diabatic stability gradient for momentum,
$= (1 - 16\zeta)^{-0.25}$ for unstable conditions,
$= 1 + 5.2\zeta$ for stable conditions.

Defining a constant C such that:

$$C = F_q(\kappa)/\kappa^{-5/3} \tag{10}$$

then:

$$E = \rho\left[\frac{\left(k(z-d_0)\right)^{2/3} R_m^{1/3}}{\Phi_{sv}\beta q}\right]^{0.5} u^* C^{0.5}. \tag{11}$$

Fluxes can also be derived from temporal data as well as spatial data. By employing Taylor's hypothesis that equates time and space ($\kappa \approx f/u$), time series information can be converted into the spatial domain by virtue of the wind velocity. This technique is often used to transform time series data obtained from standard point instruments into power spectra. The computation of temporal power spectra from time series data is achieved by the following transform:

$$\kappa F_q(\kappa) = f F_q(f/u). \tag{12}$$

Once a spatial spectrum is derived from the temporal data, then the same analysis is performed as in the regular spatial spectra using (10) and (11) to obtain fluxes. If Taylor's Hypothesis is correct, then the flux as determined from the temporal spectra should be quite similar to that derived from the spatial spectra.

A comparison of lidar-derived water vapor fluxes from vertical profiles near four of the standard meteorological instruments to the fluxes derived from those instruments throughout a day at Maricopa is seen in Fig. 5. The correlation coefficient, r^2, between the measurements is 0.78. It should be noted that the standard comparisons are 30-min averages while the lidar-derived fluxes were acquired in less than 30 s. Fig. 6 is a comparison of lidar-derived fluxes from dissipation methods across the field. The correlation coefficient, r^2, between the measurements is 0.98. The higher degree of correlation is due to the longer time averaging done on the TD scans. The time scales of the two measurements are much more closely matched in the TD scans as opposed to the vertical scans. The large degree of variability of "instantaneous" fluxes as opposed to the field average from either the point instruments or lidar is especially notable. Fig. 7 is an example of this variability across the field. This variability is consistent with a growing body of evidence that "ninety percent of the flux occurs ten percent of the time" [17]. The spatial data from the lidar indicates that much of the flux is localized in space as well as time. Examination of Fig. 6 between 1500 and 1530 h shows 15 measurements made during a period when the latent energy (water vapor) fluxes varied by as much as 200 W/m^2. The average value is however, very close to the value derived from the micrometeorological instruments. This leads again to the conclusion that flux is not uniform either temporally or spatially. Because of these differences in temporal and spatial scales, direct comparisons of lidar fluxes and point instrument fluxes are difficult. Additional information on flux techniques can be found in [18].

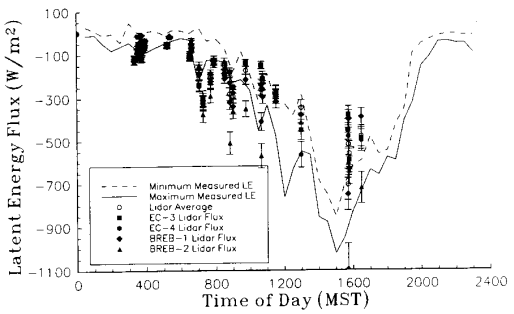

Fig. 5. Comparison of water vapor fluxes calculated from lidar vertical profiles to that derived from standard micrometeorological instruments for June 28, 1990, as a function of time of day during the MAC-V experiment. The conventional instrument comparisons are the high and low measurements made in the field at the times indicated.

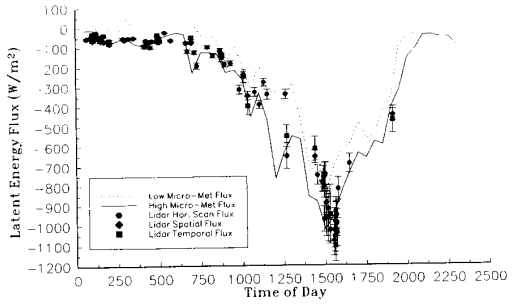

Fig. 6. Comparison of water vapor fluxes calculated from lidar spatial and temporal spectra to that derived from standard micrometeorological instruments for June 28, 1990, as a function of time of day during the MAC-V experiment. The conventional instrument comparisons are the high and low measurements made in the field at the times indicated.

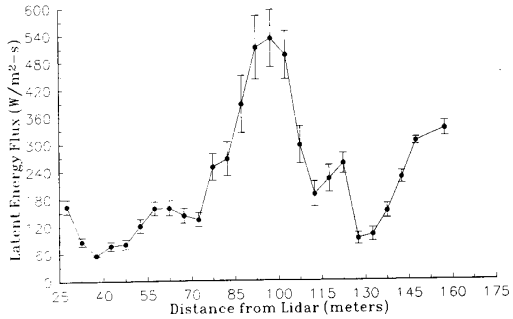

Fig. 7. The spatial variation in water vapor flux across a uniform alfalfa field as determined by the vertical profile method (10:45, June 28, 1990).

The similarity between spatial power spectra derived from spatial and temporal data as well as spectra from a number of discrete directions is remarkable. Fig. 8 is a comparison of the spatial power spectra from spatial and temporal data from a single TD scan and a spatial power spectrum from a

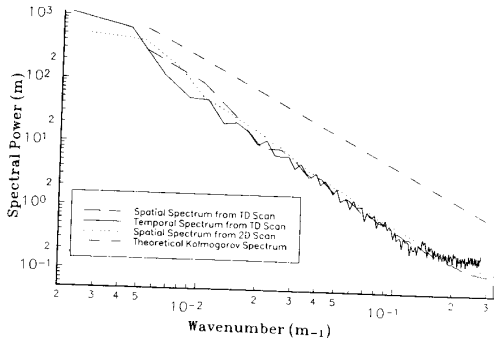

Fig. 8. Comparison of the power spectra derived from spatial and temporal data of lidar water concentrations at approximately 0730 hrs., day 180, during the MAC-V experiment. Also shown is the $-5/3$ slope predicted by Kolmogorov theory. Of special interest is the similarity between the spatial power spectra from both temporal data and spatial data and the spatial power spectrum from a horizontal scan over a wide range in directions. The actual slope is steeper than the predicted $-5/3$ because of the intermittent nature of the processes being observed [24]. The flattening of the curves at high wavenumbers is caused by aliasing of frequencies higher than the sampling rate and high frequency noise in the system.

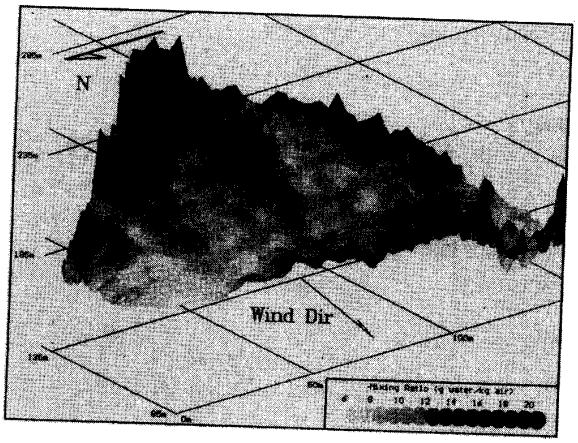

Fig. 9. Water vapor concentration over a uniform alfalfa field at 11:18, 28 June 1990 during the Maricopa experiment at an elevation of 3.2 m above the ground. The data was taken by a horizontal lidar scan over period of 2 minutes. This method enables fast, high spatial resolution data collection over relatively large areas. Of particular note is the factor of three variation in water vapor concentration (from 7 to 21-g H_2O/kg air) over an experimental field of exceptional uniformity.

horizontal scan at approximately the same time. Tennekes and Lumley [19] argue that a one-dimensional spectrum taken in an arbitrary direction cannot distinguish from a disturbance aligned with the mean wind and one oblique to it. Thus the power spectrum derived from temporal data should be different from the power spectrum derived from spatial data for arbitrary directions. The strong similarity between spectra taken in various directions was not expected. These results imply that relationships between power spectra from temporal and spatial data and thus the spatial properties of turbulence are not necessarily associated with the mean wind vector. This observation indicates that the turbulence is isotropic in the range of wavenumbers examined.

Spatial variability is found not only in fluxes but in the water vapor concentrations as well as seen in Fig. 9, an example of a horizontal scan over a uniform alfalfa field. The amount of the variability within a 100-m by 100-m field is striking considering that the field had been recently irrigated and laser leveled to ensure uniform water coverage. The point instrument array measuring fluxes also shows the same general trends. The west side of the field in Fig. 9 is drier than the southeast side, where the maximum concentrations occur. The high flux "island" structure on the north side is duplicated in both the water concentrations and flux measurements. While the details of scans throughout the day are different, the gross trends are similar. The dry parts of the field are consistently drier and the wet parts consistently wetter than the average. The traditional hypothesis of a homogeneous evaporating surface is clearly incorrect, as both the fluxes and water concentrations show little uniformity. These results challenge some of the underlying assumptions of boundary layer meteorology.

The size and distribution of the turbulent structures was evaluated using variogram analysis. Variograms related centroid to centroid (measurement point to measurement point) distance, termed lag, to the variance of the data. The variogram is a plot of the distance or lag, between measurement (x axis) and the variance of the data at a given lay (y axis) [20]. Thus it is a measure of the average variance of measurements separated by a given distance. Computationally, a variogram is the average variance minus the covariance at that lag.

A series of variograms derived from the lidar data shown in Fig. 10. The shape of the variograms give information about the distribution and sizes of the turbulent structures. A fitted Gaussian model for the structure size, the smooth lines, describe the shape reasonably well. The region of constant variability starts between 10 and 20 m range, with 50% of the variability occurring at lags of approximately 5 m. This is in agreement with characteristic lengths calculated from the integral of the autocorrelation function [10] of spatial lidar data which show lengths ranging from 3 to 7 m. These distances can be used to describe the regions of relative homogeneity and thus define the characteristic scale of turbulence. The size of the characteristic scale of turbulence (homogeneity), also suggests that the spatial sampling size must be on the same order if the fluxes and scalars of an alfalfa field are to be properly characterized. This clearly is not a reasonable option if the sampling is to be done with conventional point sensors. Not only is the cost prohibitive, but such a large number of instruments would change the characteristics of the field to be measured. This 10-m size also sets the spatial resolution required of lidar systems to do this type of analysis. In practice, oversampling by a factor of two to four is desirable to adequately characterize a signal. Thus, a 2.5-m range resolution is the maximum desirable for stable conditions with low wind speeds. In the Davis experiment, with much smaller roughness lengths, unstable atmospheric conditions and higher wind speeds the characteristic sizes were smaller by a factor of three to four. Under those conditions, the sampling size must be proportionately smaller.

The height of the plateau which represents the average variance, is a measure of the natural variations over the entire field where the larger-scale mass and energy transfer processes

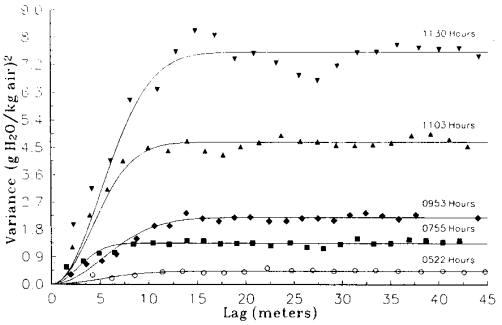

Fig. 10. Variograms of lidar-derived water concentration from various times, day 179 (June 28) 1990, during the MAC-V experiment. The solid lines represent a Gaussian distribution of structure sizes fitted to the data

begin to dominate. These include the affects of local wind patterns and advection. In examining the height of the plateau as a function of time, one finds that variations at night are small, increasing as the sun rises to a maximum near solar noon and then decreasing as the sun sets (Fig. 10). Since solar heating provides the energy which drives the turbulent transport of latent energy flux and water vapor concentration, this behavior should be expected. What was not expected is that the region of relative homogeneity (as defined by the lag at which 50% of the variability occurs) is nearly constant throughout the day. The observed variation ranges from about 4 to 7 m. It can be shown that the variances and thus the heights of the plateaus, are related through similarity theory to the water vapor flux [21].

Because of its ability to examine large areas relatively rapidly, the lidar offers an opportunity to study the concepts of stationarity and homogeneity. Stationarity refers to the assumption that the average value of the measurement (in this case, water vapor) is constant throughout the measurement. Similarly, homogeneity refers to the assumption that the average value of water vapor concentration is constant in space. These concepts assume the mathematical form

$$\frac{d\bar{q}}{dt} = 0 \quad \text{and} \quad \frac{d\bar{q}}{dx} = 0. \tag{13}$$

Terms containing these derivatives are routinely ignored when using the equations of motion. The degree to which these terms are negligible is the object of an ongoing study. Fig. 11(a) is an example of the average water concentration over a 150-m line of a sight as a function of time under unstable atmospheric conditions with a moderate wind speed. While the variations in the concentration with time can be shown to be statistically significant, at this particular time the assumption of stationarity appears to be reasonable. In contrast, Fig. 11(b) is an example of a time when the assumption clearly does not hold. Examination of the concept of homogeneity reveals similar results.

Taylor's "frozen turbulence" hypothesis is an often-used concept which allows measurements taken by conventional point instruments to be construed as spatial measurements. In this hypothesis, atmospheric structures are considered "frozen" and transported laterally by the wind. A measurement at a single point with time sees the spatial structures as they pass

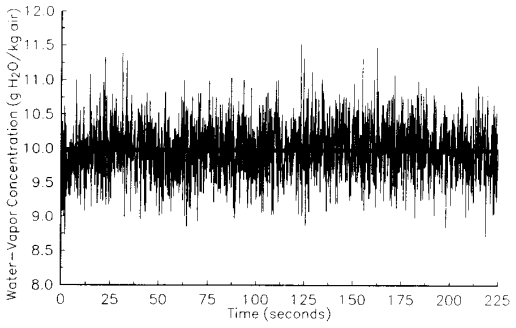

(a)

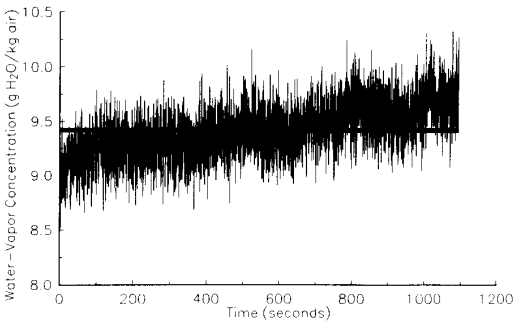

(b)

Fig. 11. Examples of the average value of the water vapor concentrations over a 150-m line of sight as a function of time. (a) shows an example of a situation where the concentration is relatively constant in time. (b) shows an example of a situation where the concentration is not constant in time and thus cannot be considered stationary.

by. The mean wind speed is used to convert the data as is done in (12). One can formulate Taylor's Hypothesis as

$$\frac{d\bar{q}}{dx} = \bar{u}\frac{d\bar{q}}{dt}.$$

The integral of the autocorrelation function is a characteristic time which can be interpreted as the average length of time it takes for a structure to pass by the detector, or in the case of the lidar, one range increment. This time can be used to estimate the sampling time required of a remote sensor to adequately capture a single structure. As one can see from Fig. 12, the characteristic time at Maricopa, under stable atmospheric conditions and low wind speeds, is about 4.9 s. To adequately sample the waveform, a sampling time of approximately 1 s per record is adequate. However, for unstable conditions, with moderate wind velocities and small structure sizes such as were present at the Davis experiment, the sampling time of 0.12 s was not adequate. The integral of the envelope of the correlation peaks in Fig. 12 is another characteristic time which is interpreted as the lifetime of a structure in the atmosphere. This is the maximum length of time over which Taylor's Hypothesis has meaning. For the case shown in Fig. 12, this time is approximately 7.6 s.

There are a series of stability correction functions used in calculations with Monin–Obulkov similarity theory ((2) and (3) for example). Measurements of these functions are difficult

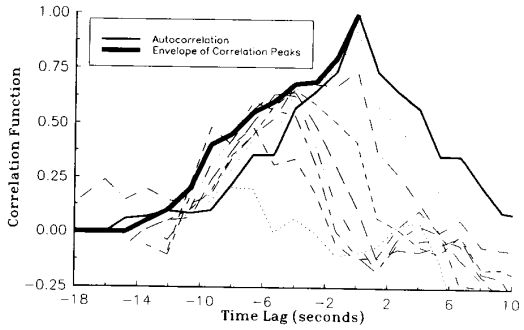

Fig. 12. Plot of the autocorrelation function and correlation functions for several distances upwind from a base distance as a function of time lag. A distance of 60-m from the lidar was chosen as the base distance. Correlation functions in time were calculated from the data taken 0, 3, 6, 9, 12, 15, 18, 21, 24, and 27 m from that base. The heavy solid line is the outer envelope of the peaks of the correlation functions. From this plot one can determine the component of the wind velocity along the line of sight, the time it takes for a structure to pass by an individual range element and the lifetime of a structure in the atmosphere. These characteristic times determine the rate at which a remote sensor must take data.

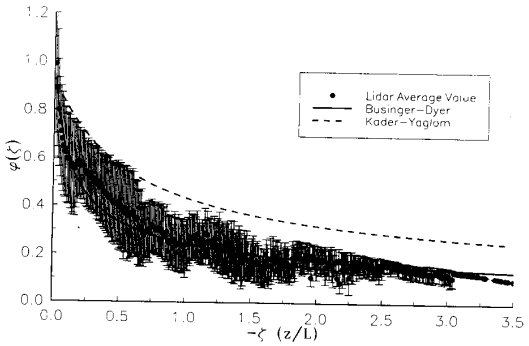

Fig. 13. Comparison of lidar-derived stability correction functions to the traditional Businger–Dyer parameterization and to the newer Kader and Yaglom parameterization. The error bars represent the standard deviations of the measurements. The small error bars on the largest values of ζ are indicative of a limited number of measurements and not necessarily decreased uncertainty.

to make because they require many vertical measurements inside the boundary layer. While a large number of parameterizations have been formulated, the community customarily uses the Businger–Dyer stability parameterization for ϕ_m and ϕ_{sv} [22]. Recently, Kader and Yaglom [23] have challenged this parameterization for the unstable case. Their formulation varies considerably, by factors of two or more for $-\zeta > 2$, from the Businger–Dyer formulation. In a single vertical scan the lidar acquires a large number of vertical measurements which can be used to determine the vertical gradient and thus the stability correction functions from the following equation:

$$\phi_{sv}(\zeta) = -\frac{[ku^*(z-d_0)\rho]}{E}\frac{d\bar{q}}{dz}.$$

Lidar measurements of the water vapor stability function were made and the results averaged over a wide range of values of ζ. Because of the very large number of measurements (greater than 41,000), an uncertainty can be calculated at each value of ζ as shown in Fig. 13. The values conform much more closely to the Businger–Dyer formulation than that of Kader and Yaglom for the range of values measured. Work continues to extend the data set to larger values of ζ and for stable atmospheric conditions.

The two-dimensional lidar measurements of water vapor concentration were made over bare soil at a spatial resolution of 1.5 m, and at sampling rates approaching 10 Hz. With this temporal and spatial resolution it should be possible to evaluate the implications of the frozen turbulence hypothesis. The two-dimensional data was processed directly into both temporal and spatial spectra for comparison and analysis. If the frozen turbulence hypothesis is correct than these spectra should match each other closely in shape and magnitude. At many times during the day, the temporal and spatial spectra do in fact resemble each other closely (Fig. 8). While this test is sufficient to evaluate the applicability of the temporal to spatial conversion, it is not a sufficient condition to prove the hypothesis.

V. Conclusion

The ability of the lidar to take measurements at points separated by as little as 1.5 m along a line-of-sight simultaneously, and rapidly scan an area offers the opportunity to study the spatial and temporal variability of water vapor concentrations with resolution never before available. It offers a nonintrusive method for characterizing conditions over various types of terrain and over relatively large areas. The integration of point and lidar measurements of land surface phenomena offer experimentalists and modelers new insights into the quantification of the spatial properties of energy balance components at the surface–atmosphere interface.

Lidars can be used to determine many of the fundamental atmospheric parameters used in micrometeorological research. The ability to measure these parameters over large areas nearly simultaneously with high spatial and temporal resolution offers a unique ability to examine many of the classical assumptions of meteorology as well as providing valuable input to traditional studies. It is this combination of lidar spatial data with the judicial application of appropriate analytical methods which will make the instrument a truly valuable resource.

Acknowledgment

The authors would like to express their appreciation to David Holtkamp, Robert Quick, Jr., Joe Tiee, Fred Archuletta, and Doug Hof, without whom the lidar would never have functioned properly and without whose assistance this work would not be possible.

References

[1] R. A. Anthes, "Enhancement of convective precipitation by mesoscale variations in vegetative covering in semiarid regions," *J. Climate and Appl. Meteor.*, vol. 23, pp. 541–554, 1989.

[2] J. F. Mahfouf, E. Richard, and P. Mascart, "The influence of soil and vegetation on the development of mesoscale circulations," *J. Climate Appl. Meteor.*, vol. 26, pp. 1483–1495, 1987.

[3] R. A. Pielke and R. Avissar, "The influence of landscape structure on local and regional climate," *Landscape Ecology*, vol. 4, no. 2/3, pp. 133–155, 1990.

[4] J. E. Tillman, "In-situ water vapor measurements in the Lyman-Alpha and infrared spectrum: Theory and components," in *Land Surface Evap-*

oration, T. J. Schmugge and J. C. Andre, Eds. New York: Springer-Verlag, 1991, pp. 313–335.
[5] D. I. Cooper, W. E. Eichinger, L. Hipps, W. Dugas, D. B. Holtkamp, R. R. Karl, and F. Barnes, "Mapping the spatial variability of latent energy fluxes and water-vapor concentrations over an agronomic field," Twentieth Conference on Agricultural and Forest Meteorology, Sept. 10–13, 1991, Salt Lake City, UT.
[6] S. Melfi, J. D. Lawrence, and M. P. McCormick, "Observation of raman scattering by water-vapor in the atmosphere," *Appl. Phys. Letters,* p. 295, 1969.
[7] J. A. Cooney, "Remote measurements of atmospheric water vapor profiles using the Raman component of laser backscatter," *J. Appl. Meteorol.,* p. 182, 1970.
[8] W. E. Eichinger, D. I. Cooper, D. E. Hof, D. B. Holtkamp, R. R. Karl, C. R. Quick, and J. J. Tiee, "Development and application of a scanning, solar-blind, water Raman-lidar," *Appl. Opt.,* in press, 1992.
[9] S. H. Melfi, D. N. Whiteman, and R. Ferrare, "Atmospheric moisture structure revealed by Raman lidar," *Optics and Photonics News,* pp. 16–18, Oct. 1991.
[10] W. Brutsaert, *Evaporation into the Atmosphere* (2nd ed.). Reidel Pub. Comp., 1984.
[11] H. A. Panofsky and J. A. Dutton, *Atmospheric Turbulence.* New York: John Wiley and Sons, 1984.
[12] C. H. Champagne, C. A. Friehe, and J. C. LaRue, "Flux measurements, flux estimation techniques, and fine scale turbulence measurements in the unstable surface layer over land," *J. Atm. Sci.,* vol. 34, pp. 515–529, 1977.
[13] A. N. Kolmogorov "The local structure of turbulence in incompressible viscous fluid for very large Reynolds numbers," *C. R. Acad. Sci. USSR,* vol. 30, pp. 301–305, 1941.
[14] S. Corrosin, "On the spectrum of isotropic temperature fluctuations in an isotropic turbulence." *J. Appl. Phys.,* vol. 22, no. 4, pp. 469–473, 1951.
[15] N. E. Busch and H. A. Panofsky, "Recent spectra of atmospheric turbulence," *Quart. J. R. Met. Soc.,* vol. 94, pp. 132–148, 1968.
[16] J. R. Garratt, "Studies of turbulence in the surface layer over water. Part II: Production and dissipation of velocity and temperature fluctuations," *Quart. J. R. Met. Soc.,* vol. 98, pp. 642–657, 1972.
[17] P. H. Caramori, P. H. Schuepp, R. L. Desjardins, and J. I. Macpherson, "Structural analysis of airborne vapor flux traces over a region," *Abstracts, Tenth Conference on Biometeorology and Aerobiology, Special Session on Hydrometeorology* (Salt Lake City, UT), Sept. 10–13, 1991, pp. 161–162, 1991.
[18] W. E. Eichinger, D. I. Cooper, D. B. Holtkamp, R. R. Karl, C. R. Quick, and J. J. Tiee, "Derivation of water-vapor fluxes from lidar measurements," accepted by *J. of Bound. Lay. Meteorology,* 1992.
[19] H. Tennekes and J. L. Lumley, *A First Course in Turbulence.* Cambridge, MA: MIT Press, 1972.
[20] J. C. Davis, *Statistics and Data Analysis in Geology,* (2nd ed.). New York: John Wiley, 1986.
[21] J. E. Tillman, "The indirect determination of stability, heat, and momentum fluxes in the atmospheric boundary layer from simple scalar variables during dry unstable conditions," *J. Appl. Meteorol.,* vol. 11, pp. 783–792, 1972.
[22] J. A. Businger, J. C. Wyngaard, Y. Izumi, and E. F. Bradley, "Flux profile relationships in the atmospheric surface layer," *J. Atm. Sci.,* vol. 28, pp. 181–189, 1971.
[23] B. A. Kader and M. Y. Yaglom, "Mean fields and fluctuation moments in unstably stratified turbulent boundary layers," *J. Fluid Mech.,* vol. 212, pp. 637–662, 1990.
[24] Z. Sorbjan, *Structure of the Atmospheric Boundary Layer.* Englewood Cliffs, NJ: Prentice-Hall, 1989.

William E. Eichinger, photograph and biography not available at the time of publication.

Daniel I. Cooper, photograph and biography not available at the time of publication.

Marc Parlange, photograph and biography not available at the time of publication.

Gabriel Katul, photograph and biography not available at the time of publication.